Heliyon 9 (2023) e15703

Contents lists available at ScienceDirect

Heliyon

journal homepage: www.cell.com/heliyon

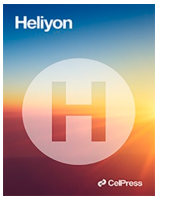

Research article

Viscoelastic hybrid nanofluid flow over a vertical plate with sinusoidal surface temperature variations

Nepal Chandra Roy *, Ayantika Ghosh

Department of Mathematics, University of Dhaka, Dhaka, 1000, Bangladesh

ARTICLE INFO

Keywords:
Viscoelastic fluid
Hybrid nanofluid
Vertical plate
Surface temperature
Magnetic field

ABSTRACT

Natural convection of a viscoelastic hybrid nanofluid along a vertically heated plate with sinusoidal surface temperature variations is investigated. The current investigation explores the non-similar boundary layer flow patterns and heat transfer of second-grade viscoelastic flow of hybrid nanofluid. Effects of magnetic field and thermal radiation are considered. The governing dimensional equations are converted into a non-dimensional form taking suitable transformations. Resulting equations are solved with the aid of finite difference method. It is discovered that the momentum boundary layer lessens while the thermal boundary layer grows for higher radiation parameters, surface temperature parameters, Eckert numbers, magnetic field parameters and amount of nanoparticles. For larger Deborah numbers (De_1), shear stress (τ) and heat transfer rate (q) accelerate, but momentum and thermal boundary decline near the leading edge of the vertical plate. However, the effects of Deborah number (De_2) show opposite results. Increase in magnetic field parameters causes a reduction in shear stress. The higher volume fraction of nanoparticles (φ_1, φ_2) enhances q as it was expected. Moreover, τ and q were increased with larger surface temperature parameters and decrease with higher Eckert numbers. This is because higher surface temperature boost up the fluid temperature, but higher Eckert numbers admit the fluid to spread over the surface. An increase in the amplitude of surface temperature oscillation enhances the shear stress and heat transfer rate.

1. Introduction

Second-grade viscoelastic fluid has received the attraction of researchers due to its outstanding practical utilizations including automotive coolant, array of heaters, gas burner, heat exchangers, coolant of microchips. In 1963, Beard and Walters [1] researched the stagnation point flow of viscoelastic fluid. Results showed that increasing in elasticity parameter increased fluid velocity near the boundary layer. Later, Davies [2] theoretically discussed the findings of Beard and Walters [1]. Second-grade fluid flow near the boundary of a stretched sheet was analytically investigated by Vajravelu and Rollins [3]. Turkyilmazoglu [4] also theoretically analyzed the convective flow of a magnetohydrodynamic (MHD) viscoelastic fluid over a permeable stretched sheet. They discussed results for Walters-B liquid and second grade fluid. The peristaltic flow of a second-grade fluid was investigated by Hameed et al. [5]. The modified second-grade fluid flow along a non-linear stretched sheet was conducted by Khan and Rahman [6]. Results revealed that for larger second grade fluid parameter velocity increases while temperature profiles showed the opposite. Salahuddin et al. [7] discussed the viscoelastic fluid flow showing the impact of some thermo-physical parameters along a stretching surface.

* Corresponding author.
E-mail address: nepal@du.ac.bd (N.C. Roy).

https://doi.org/10.1016/j.heliyon.2023.e15703
Received 20 December 2022; Received in revised form 11 April 2023; Accepted 19 April 2023
Available online 26 April 2023

Nomenclature

$\widetilde{x},\widetilde{y}$	Coordinate axes (Dimensional) (m)
x, y	Coordinate axes (Dimensionless)
L	Length of the plate (m)
$\widetilde{u},\widetilde{v}$	Velocity component (Dimensional) (m/s)
u,v	Velocity component (Dimensionless)
g	Gravitational acceleration (m/s^2)
$\widetilde{T}$	Temperature (K)
T_∞	Ambient temperature (K)
T_w	Surface mean temperature (K)
B_0	Strength of magnetic field (kg/s^{2}A)
MHD	Magnetohydrodynamic
Gr_L	Grashof number
c_p	Capacity of heat (J/KgK)
k	Thermal conductivity (W/mK)
De	Deborah number
Ec	Eckert number
Pr	Prandtl number
M	Magnetic parameter
Δ	Surface temperature parameter
Rd	Radiation conduction parameter
q	Heat transfer rate
a	Amplitude of surface temperature variations (m)

Greek symbols

ψ	Stream function
α	Thermal diffusivity (m^2/s)
β	Thermal expansion coefficient (1/K)
ρ	Density (kg/m^3)
μ	Absolute viscosity (Ns/m^2)
ν	Kinematic viscosity (m^2/s)
σ	Electrical conductivity (A^{2}s^3/kgm^2)
$\rho\beta$	Coefficient of volumetric expansion
θ	Dimensionless temperature
δ	Boundary layer
τ	Shear stress
φ	Volume fraction

Superscript

(')	Differentiation with respect to Y

Subscript

Cu	Cu nanoparticles
Fe_3O_4	Fe_3O_4 nanoparticles
f	Base fluid
hnf	Hybrid nanofluid
M	Momentum boundary
T	Thermal boundary
w	Condition at the surface
∞	Circumstances for being far away from the surface

Heat transfer of fluids is significant from a technical point of view. Usually, base fluids were considered for heat transfer analysis. However, there is limitation in heat transfer of base fluids because of low thermal conductivity. To overcome such a type of limitation Choi [8] first discovered the concept of nanofluids. Nanofluids are prepared by mixing nanoparticles into the conventional fluids (water, kerosene, oil, ethylene glycol). Studies have shown that nanofluids show better thermal performance compared to base fluids. It has many applications, such as, heat exchanger, refrigerator, nano-sized electronics, bio-technology, and chemical engineering. Numerous authors [9–12] reported the improvement of the heat transfer rate of nanofluids in their respective literatures. Grosan and Pop [13] illustrated the heat transport of nanofluids on a biaxial stretched sheet. They achieved dual solutions and performed stability analysis for the different values of pertinent fluid parameters including suction parameters, stretching parameters, Prandtl numbers

and Schmidt numbers. They did not take thermal diffusion into account. Anuar et al. [14] have analyzed MHD flow considering the inclusion of carbon nanotubes in kerosene oil and water. Tian et al. [15] numerically elucidated a non-Newtonian stagnation flow of fluid along a stretched surface. They have solved the presented equations by the collocation spectral scheme and considered the magnetic Brownian motion effect. Narahari et al. [16] studied flow of multiphase nanofluids on a vertical plate due to steady heat flux. In their literature, they solved the respective equations by Crank-Nicolson scheme. They showed the results graphically with the impacts of several fluid parameters on temperature, velocity, local Nusselt number, and average skin-friction. Results reviewed that, the ratio of buoyance parameters did not exhibit any impact on the regional Nusselt number profiles.

In the above literature, we addressed study articles based on nano-fluids. In recent time, a fluid has gained the attention of numerous researchers in the case of its fastest heat transport rate. The name of that type of fluid is hybrid nanofluid. It is obtained by mixing two types of nanoparticles into conventional fluids. Hussein et al. [17] had examined the heat transfer augmentation of fluids by dissolving hybrid nanoparticles in base fluid (ethylene glycol). Lund et al. [18] investigated stability analysis on hybrid nanofluid along a shrinking surface. They also taken the participation of viscous dissipation. For the smallest eigenvalue the first solution was stable compared with the second solution. Zainal et al. [19] explored the role of magnetic parameters on hybrid nanofluid along a vertical plate. Consequences showed that, the velocity increased with larger magnetic field parameters, but the temperature profiles showed opposite character. Junoh et al. [20] demonstrated hybrid nanofluid flow that passes a shrinking sheet. They quantitatively solved the presented equations using MATLAB and plotted the result graphically based on dual solutions. Compared to nanofluids, hybrid nanofluids had decreased skin friction, but increased heat transport rate. In the published literatures [21–30] numerous researchers did their work based on nanofluid and hybrid nanofluid considering convective heat transfer and different shapes of geometry.

Fluids that obey the Newton's law (that is, fluids with constant viscosity) are known well by Newtonian fluids. Because no base fluid abides by the law, Newtonian fluids are utilized for practical purposes based on assumptions. The definition of non-Newtonian fluid came from Newtonian fluid. In our present research we consider three types of non-Newtonian fluids, Maxwell, Jeffrey, and Oldroyd-B fluid, because of their too many practical interest. Several authors regarded the impacts of different fluid parameters on that types of fluids and showed the effective results graphically.

Nisar et al. [31] analytically solved the MHD convective flow under the effects of chemical reactions using the Adomian Decomposition Method (ADM). Over a stretching sheet, Ahmad and Ishak [32] considered Jeffrey fluid flow considering porous medium. Consequences showed that, heat transfer decreased for higher magnetic field parameters while increased for higher Prandtl number. The flow of Jeffrey fluid under the consideration of an endoscope was conducted by Hayat et al. [33]. Alsaedi et al. [34] developed the exact solution of Jeffrey fluid where the boundary conditions were convective. They also took the consideration mass and heat transfer with chemical reactions and showed that the exact solutions agreed with numerical solutions. On the other side, Turkyilmazoglu and Pop [35] analytically derived the exact solutions of Jeffrey fluid towards a stretched sheet.

Maxwell fluid is a special case of non-Newtonian fluid that is closely connected with relaxation time. Recently, Haneef et al. [36] mathematically delimitated the heat transfer of Maxwell fluid with try or hybrid nanoparticles. Hanif [37] mathematically described the fractional Maxwell fluid flow using the aid of Crank-Nicolson method and found that the temperature profiles showed opposite characters with Prandtl number. The magnetite dipole effect on Maxwell fluid along a stretched sheet was researched by Kumer et al. [38] and Jamshed [39] considered the MHD effect on Maxwell nanofluid. Zhang et al. [40] and Khan et al. [41] studied natural convection on Maxwell fluid flow. They [40] performed the comparison between thermal transport and Prabhakar fractional free convection. On the other side, Khan et al. [41] performed simulation procedures of Prabhakar fractional Maxwell fluid. Fetecau and Fetecau [42] determined two appropriate solutions of Maxwell fluid flow over an infinitely flat plate. Their investigation concluded that, the solutions had distinct algebraic structure, but the numerical values corresponding to the solutions were found to be identical.

Haneef et al. [43] explored the thermal enhancement of Oldroyd-B hybrid nanofluids in the appearance of mass transfer by using Cattanio-Christov (CC) heat flux theory. They graphically plotted the results showing the effects of using nanofluid and hybrid nanofluid on temperature profiles. Using hybrid nanofluids showed better performance than nanofluids. By using the same (CC) theory, Hayat et al. [44] investigated Oldroyd-B nano-fluid flow along a stagnation point. The MHD Oldroyd-B fluid flow was investigated by Hina et al. [45] in two contiguous directions. Awan et al. [46] examined how Oldroyd-B fluid flowed electro-osmotically between two plates. The fluid velocity boosted up for improving values of slip parameters but slowed down for upper values of pressure gradient. Liu et al. [47] showed the exact analytical solution of Couette flow of Oldroyd-B fluid in sight of magnetic field with fractional derivative. Ibrahim and Gadisa [48] considered the non-linear Oldroyd-B fluid flow along a non-linear stretched sheet with the effects of heat absorption. The differential equations were solved by the Galerkin finite element method. They graphically showed the results for different fluid parameters and stretching parameters.

To seek the impacts of thermal radiation on heat transport of several fluids has enormous applications in fluid dynamics. Several authors have considered the influences of thermal radiation in their respective literatures for getting better thermal performance. Qasim [49] considered the influences of emerging parameters to determine the rate of heat transport of Jeffrey fluid along a stretching sheet. It was found that the velocity profiles showed its increasing character while the temperature profile declined with an increment of Deborah number. The impacts of radiation on natural convection was investigated by Mahfooz and Hossain [50]. Shehzad et al. [51] studied the thermophoresis effects on MHD radiative Jeffrey fluid along a stretched surface. They derived series solutions for concentration, temperature, and velocity profiles. Aydm and Kaya [52] showed the impacts of radiation on MHD fluid flow over a vertical plate in the case of mixed convection. It was viewed that, an increase in radiation parameter heat transfer coefficients increased, but local skin friction coefficients were found to be decreased. Rashidi et al. [53] investigated heat transfer on free convection for MHD fluid along a vertically stretched surface. They considered the effects of radiation and analytically solved the presented governing equations. Wang et al. [54] studied the heat transportation of a non-Newtonian fluid with a radiative heat flux on a convectively heated

surface. Wakif et al. [55] examined the impacts of thermal radiation on MHD hybrid nano-fluid using the Buongiorno's nanofluid model. They performed stability analysis on convection cells and carried out excellent results. The authors [56–59] also considered the impacts of thermal radiation in their representative literatures.

The influences of surface temperature on boundary layer along a vertically heated surface in streamwise direction was discussed by Rees [60]. Result reviewed that, the numerical investigation agreed with the asymptotic results. Then Roy and Hossain [61] utilized the results from Rees [60] and numerically showed the effects on variations of concentration and streamwise temperature on free convection flow. After that, Molla et al. [62] quantitatively examined the effects of radiation parameters on natural convection in terms of variations of sinusoidal surface temperature along a vertical plate. It was identified that, the heat transfer and skin friction became the growing function of radiation parameter. Chen et al. [63] derived the solution of natural convection flow in four different methods and showed that the four solutions were in good agreement. Ghaffari et al. [64] mathematically analyzed the rate of heat transfer owing to sinusoidal wall temperature along an oscillating stretched surface. They plotted the streamlines and isotherm profiles for different pertinent fluid parameters. An increase of Prandtl number enhanced the heat transport rate. Roy [65] discussed the MHD flow of a nanofluid assuming the variations of sinusoidal surface temperature. It was concluded that, along the streamwise direction the heat transport rate increased while the shear stress decreased.

The aforementioned literature review indicates that viscoelastic second-grade fluid flow along a vertical plate with a magnetic field along with thermal radiation is impressive with boundary layer characteristics because of its frequent occurrence in practical purposes. Most studies considered streamwise variations boundary conditions. However, similarity transformations were used to analyze the problems. It might not always be true that the profiles will be symmetric along the streamwise direction. In this case, non-similar transformations must be used. Here sinusoidal surface temperature variations have been considered. So the goal of current investigation is to explore the non-similar boundary layer flow patterns and heat transport of second-grade viscoelastic flow of hybrid nanofluid along a vertically heated plate in the company of thermal radiation and magnetic field owing to variations of sinusoidal surface temperature. Finite difference method was used to solve the presented governing equations. Outcomes were represented with streamlines and isotherms, and rate of heat transfer, and skin friction varying the physical parameters.

2. Mathematical formulation

Along a vertical plate, a steady two-dimensional viscoelastic flow of hybrid nanofluid is taken with variations of sinusoidal surface temperature. The current structure of the flow is drawn in Fig. 1. Here $\tilde{x}$ indicates the expected length from the leading corner of the plate, $\tilde{y}$ is the expected length from the plane which is directed orthogonal to $\tilde{x}$, the characteristic length is symbolized by L. Table 1 depicts the thermo-physical quantities of nanoparticles and water. The boundary layer equations for mass, momentum and energy [1]

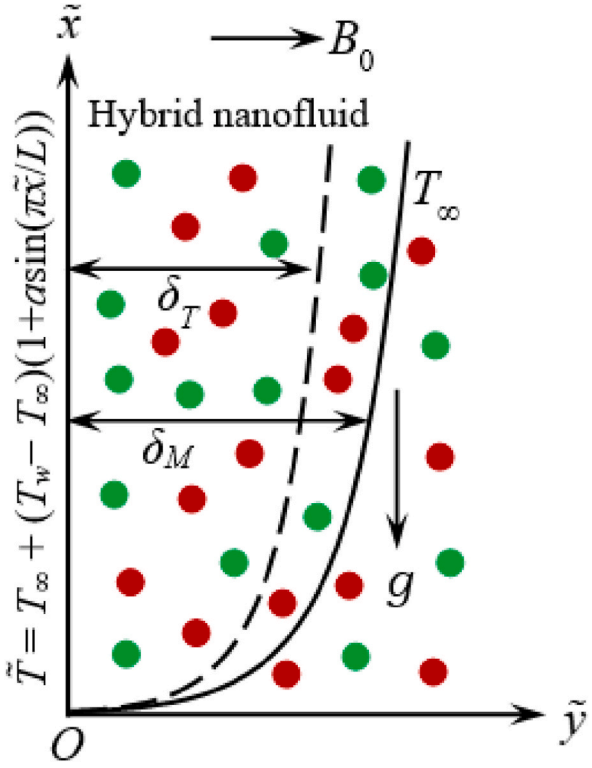

Fig. 1. Geometry of the problem.

are

$$\frac{\partial \widetilde{u}}{\partial \widetilde{x}}+\frac{\partial \widetilde{v}}{\partial \widetilde{y}}=0 \tag{1}$$

$$\begin{aligned}&\widetilde{u}\frac{\partial \widetilde{u}}{\partial \widetilde{x}}+\widetilde{v}\frac{\partial \widetilde{u}}{\partial \widetilde{y}}=\frac{\mu_{hnf}}{\rho_{hnf}}\frac{\partial^2 \widetilde{u}}{\partial \widetilde{y}^2}-\frac{\alpha_1}{\rho_{hnf}}\left(\widetilde{u}\frac{\partial^3 \widetilde{u}}{\partial \widetilde{x}\partial \widetilde{y}^2}-\frac{\partial \widetilde{u}}{\partial \widetilde{y}}\frac{\partial^2 \widetilde{u}}{\partial \widetilde{x}\partial \widetilde{y}}+\widetilde{v}\frac{\partial^3 \widetilde{u}}{\partial \widetilde{y}^3}+\frac{\partial \widetilde{u}}{\partial \widetilde{x}}\frac{\partial^2 \widetilde{u}}{\partial \widetilde{y}^2}\right)\\&-\alpha_2\left[\widetilde{u}^2\frac{\partial^2 \widetilde{u}}{\partial \widetilde{x}^2}+2\widetilde{u}\widetilde{v}\frac{\partial^2 \widetilde{u}}{\partial \widetilde{x}\partial \widetilde{y}}+\widetilde{v}^2\frac{\partial^2 \widetilde{u}}{\partial \widetilde{y}^2}\right]+\frac{g(\rho\beta)_{hnf}}{\rho_{hnf}}(\widetilde{T}-T_\infty)-\frac{\sigma_{hnf}}{\rho_{hnf}}B_0^2\left(\widetilde{u}+\alpha_2\widetilde{v}\frac{\partial \widetilde{u}}{\partial \widetilde{y}}\right),\end{aligned} \tag{2}$$

$$\widetilde{u}\frac{\partial \widetilde{T}}{\partial \widetilde{x}}+\widetilde{v}\frac{\partial \widetilde{T}}{\partial \widetilde{y}}=\alpha_{hnf}\frac{\partial^2 \widetilde{T}}{\partial \widetilde{y}^2}-\frac{1}{(\rho C)_{hnf}}\frac{\partial q_r}{\partial \widetilde{y}}+\frac{\sigma_{hnf}}{(\rho C)_{hnf}}B_0^2\widetilde{u}^2+\frac{\mu_{hnf}}{(\rho C)_{hnf}}\left(\frac{\partial \widetilde{u}}{\partial \widetilde{y}}\right)^2, \tag{3}$$

with appropriate boundary conditions [60].

$$\widetilde{u}=\widetilde{v}=0,\widetilde{T}-T_\infty=(T_w-T_\infty)(1+a\sin(\pi\widetilde{x}/L)),\text{at }\widetilde{y}=0,\widetilde{u}=0,\widetilde{T}=T_\infty\text{ as }\widetilde{y}\to\infty \tag{4}$$

Here, $\widetilde{a}$ and $\widetilde{v}$ are addressed as the components of fluid velocity in the $\widetilde{x}$- direction and $\widetilde{y}$-direction, $\widetilde{T}$ refers the steady temperature inside the boundary layer, T_∞ is ambient temperature, and T_w is the surface mean temperature. Furthermore, β, stands for thermal expansion coefficient, ν, stands for kinematic viscosity, g, stands for gravitational acceleration, α_1, and α_2 are material constants associated to second-grade fluid, B_0 presents the power of the magnetic field and orthogonal to the vertical plate, the amplitude of variations of surface temperature variations is symbolized by a and the expected wave length of fluctuations is $2L$.

The necessity quantities of hybrid nanofluids are presented below:

$$\mu_{hnf}=\frac{\mu_f}{(1-\varphi_{hnf})^{2.5}},\varphi_{hnf}=\varphi_{Fe_3O_4}+\varphi_{Cu},\rho_{hnf}=\varphi_{Fe_3O_4}\rho_{Fe_3O_4}+\varphi_{Cu}\rho_{Cu}+(1-\varphi_{hnf})\rho_f,$$

$$\alpha_{hnf}=\kappa_{hnf}\Big/(\rho c)_{hnf},(\rho c)_{hnf}=\varphi_{Fe_3O_4}(\rho c)_{Fe_3O_4}+\varphi_{Cu}(\rho c)_{Cu}+(1-\varphi_{hnf})(\rho c)_f,$$

$$\frac{\kappa_{hnf}}{\kappa_f}=\frac{(\kappa_{np}+2\kappa_f)-2\varphi(\kappa_f-\kappa_{np})}{(\kappa_{np}+2\kappa_f)+\varphi(\kappa_f-\kappa_{np})},\kappa_{np}=\frac{\varphi_{Fe_3O_4}\kappa_{Fe_3O_4}+\varphi_{Cu}\kappa_{Cu}}{\varphi_{Fe_3O_4}+\varphi_{Cu}},$$

$$(\rho\beta)_{hnf}=\varphi_{Fe_3O_4}(\rho\beta)_{Fe_3O_4}+\varphi_{Cu}(\rho\beta)_{Cu}+(1-\varphi_{hnf})(\rho\beta)_f,$$

$$\frac{\sigma_{hnf}}{\sigma_f}=\frac{(\sigma_{np}+2\sigma_f)-2\varphi(\sigma_f-\sigma_{np})}{(\sigma_{np}+2\sigma_f)+\varphi(\sigma_f-\sigma_{np})},\sigma_{np}=\frac{\varphi_{Fe_3O_4}\sigma_{Fe_3O_4}+\varphi_{Cu}\sigma_{Cu}}{\varphi_{Fe_3O_4}+\varphi_{Cu}},$$

here ρ_f, indicates the density, μ_f, refers the effective dynamic viscosity, σ_f and κ_f are refer the electrical and thermal conductivity, c_f indicates the heat capacity, the volumetric expansion coefficient of conventional fluid is $(\rho\beta)_f$. The similar expressions for hybrid nanofluid are denoted by the subscript *hnf*. Again, the subscripts Fe_3O_4 and Cu refer to the volumes of the Fe_3O_4 and Cu nanoparticles.

To make the calculations easier, the leading Eq. (1)–(4) are designed to reduce into non-dimensional form by using the following dimensionless variables:

$$\widetilde{u}=\nu_f Gr_L^{1/2}u\Big/L,\widetilde{v}=\nu_f Gr_L^{1/4}v\Big/L,T=(\widetilde{T}-T_\infty)/(T_w-T_\infty),\widetilde{x}=xL,\widetilde{y}=yLGr_L^{-1/4}. \tag{5}$$

Here $Gr_L=g\beta q_0L^4/(\kappa_f\nu_f^2)$ indicates the local Grashof number.

Combining Eq. (5) and Eq. (2)–(4), we obtain

Table 1
Thermo-physical quantities of based fluid and nano-sized particles [66,67].

Quantities	Base fluid (H_2O)	Cu	Fe_3O_4
c ($Jkg^{-1}K^{-1}$)	4179	385	670
ρ (kgm^{-3})	997.1	8933	5180
κ ($Wm^{-1}K^{-1}$)	0.613	401	9.7
$\beta\times10^{-5}$ (K^{-1})	21	1.67	1.3
σ $m\Omega^{-1}$	0.05	5.96×10^7	2.50×10^4

$$u\frac{\partial u}{\partial x}+v\frac{\partial u}{\partial y}=\frac{\mu_{hnf}}{\mu_f}\frac{\rho_f}{\rho_{hnf}}\frac{\partial^2 u}{\partial y^2}-\frac{\rho_f}{\rho_{hnf}}De_1\left(u\frac{\partial^3 u}{\partial x\partial y^2}-\frac{\partial u}{\partial y}\frac{\partial^2 u}{\partial x\partial y}+v\frac{\partial^3 u}{\partial y^3}+\frac{\partial u}{\partial x}\frac{\partial^2 u}{\partial y^2}\right)$$
$$-De_2\left[u^2\frac{\partial^2 u}{\partial x^2}+2uv\frac{\partial^2 u}{\partial x\partial y}+v^2\frac{\partial^2 u}{\partial y^2}\right]+\frac{(\rho\beta)_{hnf}}{(\rho\beta)_f}\frac{\rho_f}{\rho_{hnf}}T-\frac{\sigma_{hnf}}{\sigma_f}\frac{\rho_f}{\rho_{hnf}}M\left(u+De_2v\frac{\partial u}{\partial y}\right), \tag{6}$$

$$u\frac{\partial T}{\partial x}+v\frac{\partial T}{\partial y}=\frac{1}{\mathrm{Pr}}\frac{\alpha_{hnf}}{\alpha_f}\left\{1+\frac{4}{3}\frac{k_f}{k_{hnf}}R_d(1+\Delta T)^3\right\}\frac{\partial^2 T}{\partial y^2}$$
$$+\frac{4}{\mathrm{Pr}}\frac{(\rho C)_f}{(\rho C)_{hnf}}\Delta R_d(1+\Delta T)^2\left(\frac{\partial T}{\partial y}\right)^2+\frac{\sigma_{hnf}}{\sigma_f}\frac{(\rho C)_f}{(\rho C)_{hnf}}EcMu^2+\frac{\mu_{hnf}}{\mu_f}\frac{(\rho C)_f}{(\rho C)_{hnf}}Ec\left(\frac{\partial u}{\partial y}\right)^2, \tag{7}$$

with reduced boundary conditions,

$$u=v=0, T=1+a\sin(\pi x) \text{ at } y=0, u=0, T=0 \text{ as } y\to\infty \tag{8}$$

in Eqs. (6) and (7), the parameters are defined by

$$De_1=\frac{\alpha_1 Gr_L^{1/2}}{\rho_f L^2}, De_2=\frac{\alpha_2\nu_f Gr_L^{1/2}}{L^2}, \mathrm{Pr}=\frac{\nu_f}{\alpha_f}, M=\frac{B_0^2L^2\sigma_f}{\rho_f\nu_f Gr_L^{1/2}}, \Delta=\frac{T_w-T_\infty}{T_\infty},$$
$$Ec=\frac{\nu_f^2 Gr_L}{c_f L^2(T_w-T_\infty)}, Rd=\frac{4\sigma T_\infty^3}{k_f k^*}.$$

Here, Pr indicates the Prandtl number, De_1 and De_2 are Deborah numbers, M refers the magnetic parameter, Rd is the radiation parameter, Δ is the surface temperature parameter, and Ec is the Eckert number.

Stream function formulation is introduced here as,

$$\psi=X^{\frac{3}{4}}f(X,Y), T=\theta(X,Y), X=x, Y=yX^{-\frac{1}{4}} \tag{9}$$

Using Eq. (9), the system of equations (6)–(8) reduces to

$$\frac{\mu_{hnf}}{\mu_f}\frac{\rho_f}{\rho_{hnf}}f'''+\frac{3}{4}ff''-\frac{1}{2}f'^2+\frac{(\rho\beta)_{hnf}}{(\rho\beta)_f}\frac{\rho_f}{\rho_{hnf}}\theta-Dex_1\left(\frac{1}{2}f'f'''-\frac{1}{4}f''^2-\frac{3}{4}ff^{iv}\right)-Dex_2\left(\frac{3Y}{16}f'^2f''-\frac{1}{4}f'^3-\frac{3}{8}ff'f''+\frac{9}{16}f^2f'''\right)-\frac{\sigma_{hnf}}{\sigma_f}\frac{\rho_f}{\rho_{hnf}}M\left(X^{\frac{1}{2}}f'+Dex_2\right.$$
$$\left.\left(\frac{3}{4}ff''-\frac{Y}{4}f'f''+Xf''\frac{\partial f}{\partial X}\right)\right)=X\left[\left(f'\frac{\partial f'}{\partial X}-f''\frac{\partial f}{\partial X}\right)+Dex_1\left(f'\frac{\partial f'''}{\partial X}+f'''\frac{\partial f'}{\partial X}-\right.\right.$$
$$f''\frac{\partial f''}{\partial X}-f^{iv}\frac{\partial f}{\partial X}\Big)+Dex_2\left(f'^2\frac{\partial f'}{\partial X}-\frac{3}{2}ff'\frac{\partial f''}{\partial X}-\frac{1}{2}f'f''\frac{\partial f}{\partial X}+\frac{3}{2}ff'''\frac{\partial f}{\partial X}\right)+$$
$$\left.X\left(f'^2\frac{\partial^2 f'}{\partial X^2}-2f'\frac{\partial f}{\partial X}\frac{\partial f''}{\partial X}+f'''\left(\frac{\partial f}{\partial X}\right)^2\right)\right], \tag{10}$$

$$\frac{1}{\mathrm{Pr}}\frac{\alpha_{hnf}}{\alpha_f}\left\{1+\frac{4}{3}\frac{k_f}{k_{hnf}}R_d(1+\Delta\theta)^3\right\}\theta''+\frac{3}{4}f\theta'+\frac{4}{\mathrm{Pr}}\frac{(\rho C)_f}{(\rho C)_{hnf}}\Delta R_d(1+\Delta\theta)^2\theta'^2+$$
$$\frac{\sigma_{hnf}}{\sigma_f}\frac{(\rho C)_f}{(\rho C)_{hnf}}EcMXf'^2+\frac{\mu_{hnf}}{\mu_f}\frac{(\rho C)_f}{(\rho C)_{hnf}}EcX^{\frac{1}{2}}f''^2=X\left(f'\frac{\partial\theta}{\partial X}-\theta'\frac{\partial f}{\partial X}\right), \tag{11}$$

here, $Dex_1=\frac{\rho_f}{\rho_{hnf}}X^{-\frac{1}{2}}De_1, Dex_2=X^{-\frac{1}{2}}De_2,$.

with transformed boundary conditions:

$$f=f'=0, \theta=1+a\sin(\pi X) \text{ at } Y=0, f=0, \theta=0, \text{as } Y\to\infty \tag{12}$$

in Eq (10)–(12), f' indicates the differentiation of the function $f(X,Y)$ with respect to Y.

The significant quantities of physical interests are the shear stress τ, and the heat transfer rate, q, are given by,

$$\widetilde{\tau}=\left[\mu_{hnf}\frac{\partial\widetilde{u}}{\partial\widetilde{y}}-\alpha_1\left(u\frac{\partial^2\widetilde{u}}{\partial\widetilde{x}\partial\widetilde{y}}+v\frac{\partial^2\widetilde{u}}{\partial\widetilde{y}^2}+2\frac{\partial\widetilde{u}}{\partial\widetilde{x}}\frac{\partial\widetilde{u}}{\partial\widetilde{y}}\right)\right]_{\widetilde{y}=0} \text{and}, \widetilde{q}=-\left(\kappa_{hnf}\frac{\partial\widetilde{T}}{\partial\widetilde{y}}-q_r\right)_{\widetilde{y}=0}. \tag{13}$$

Using equations (5) and (9) into equation (13), the non-dimensional quantities of Eq. (13) are

$$\tau=X^{\frac{1}{4}}\left[\frac{\mu_{hnf}}{\mu_f}f''+De_1X^{\frac{1}{2}}\left(2f''\frac{\partial f'}{\partial X}-f'''\frac{\partial f}{\partial X}\right)\right]_{\eta=0} \text{and}, q=\left[\left\{\frac{k_{hnf}}{k_f}+\frac{4}{3}Rd(1+\Delta\theta)^3\right\}\theta'\right]_{\eta=0},$$

where, $\tau = \frac{\widetilde{\tau}L^2}{\nu_f \mu_f Gr_L^{3/4}}$ and $q = \frac{\widetilde{q}L}{k_f(T_w - T_\infty)Gr_L^{1/4}}$.

3. Solution methodology

The equations (10) and (11) give a system of Eqs. with boundary conditions (12). The system of Eqs. is solved by the aid of finite difference method. When it is tough to find an analytical solutions of a system of equations then finite difference method is applied to solve them. Higher order accuracy can be easily obtained by using this method. Initially, by assuming $V = f$ and $U = f'$ Eqs. (10) and (11) are transformed to a system of second order differential equations. To discretize the obtained resulting equations, a backward difference scheme is applied in X-direction and a central difference scheme is applied in Y-direction. As a result, a tri-diagonal system of algebraic Eqs. of the following type is generated:

$$P_k F_{m-1,n} + Q_k F_{m,n} + R_k F_{m+1,n} = W_k, \tag{15}$$

where k (= 1 and 2) presents U and θ respectively, the grid points in Y and X directions are m (= 1, 2, 3, …, m_x) and n (= 1, 2, 3, …, n_x) respectively. Fixing n, the tri-diagonal Eq. (15) for m (= 1, 2, 3, …, m_x) are solved by Thomas Algorithm [68]. The solutions converge when the difference between two successive iterations is less than 10^{-6}. The step sizes ΔX and ΔY are used to partition the domain (X, Y). These are set at $\Delta X = 0.002$ and $\Delta Y = 0.0005$ in order to maintain the grid independence of the solutions.

4. Results and discussion

Fig. 2 exhibits a comparison between current results and Beard and Walters [1]. It should be emphasized that the velocity profile is generated using the boundary conditions proposed by Beard and Walters [1] considering $De_1 = De_2 = \varphi_1 = \varphi_2 = \Delta = Ec = Rd = a = M = 0$. Fig. 2 clearly shows that the two outcomes are in excellent agreement.

Fig. 3(a)-(b) describe the effects of Deborah number, De_1, on τ and q. With an increase in De_1, τ increases slowly, however, in case of $De_1 = 0.1$ and $De_1 = 0.2$ small changes are found. From Fig. 3(b), the changes in heat transfer show little change with the increase of De_1.

Fig. 4(a)-(b) explain the influence of Deborah number, De_2, on τ and q. We have considered three different values of De_2, these are, $De_2 = 0.0$, $De_2 = 0.3$ and $De_2 = 1.0$. The increasing values of De_2, slow down both τ and q. Because, increasing of De_2, diminish fluid velocity and τ.

The impacts of amplitude of surface temperature variations, a, on τ and q for several increasing values of a shown in Fig. 5(a)-(b). When $a = 0.0$, the surface temperature remains constant, that is, no oscillation happens. The results are clearly observed in Fig. 5(a) and (b). But for improving values of a, τ oscillates slowly, whereas, q oscillates rapidly. Higher amplitude of surface temperature makes the surface an oscillating surface.

The effects of surface temperature parameters, Δ, on τ and q are elucidated in Fig. 6(a)-(b). For different increasing values of Δ, τ increases with an increase in X. On the other side, q attains its maximum at the leading edge, and decreases its value with the increase in X. Also higher Δ augments q. This is because, when surface temperature is higher, ambient temperature is less than surface

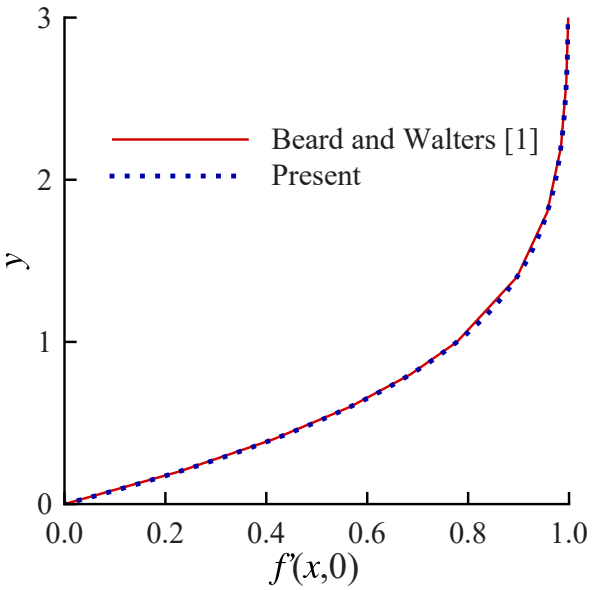

Fig. 2. Comparison between the current result and Beard and Walters [1].

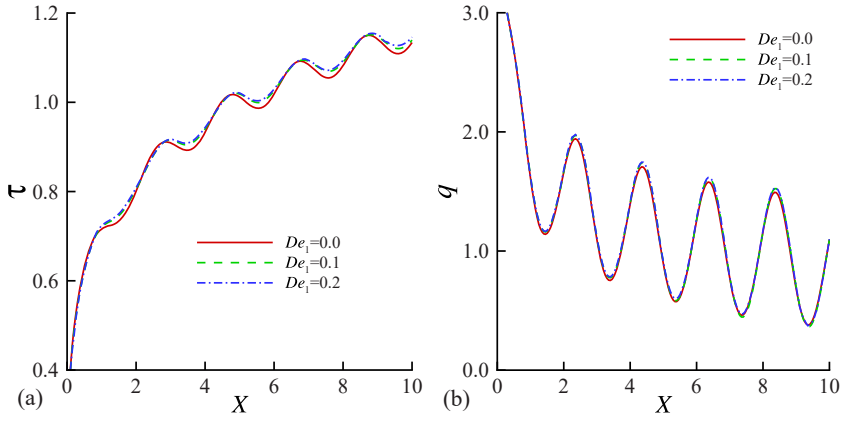

Fig. 3. (a) τ and (b) q for higher De_1, when Pr = 6.2, $a = 0.1$, $\varphi_1 = 0.05$, $\varphi_2 = 0.05$, $De_2 = 0.2$, $\Delta = 0.5$, $Ec = 0.1$, $Rd = 0.5$, and $M = 0.05$.

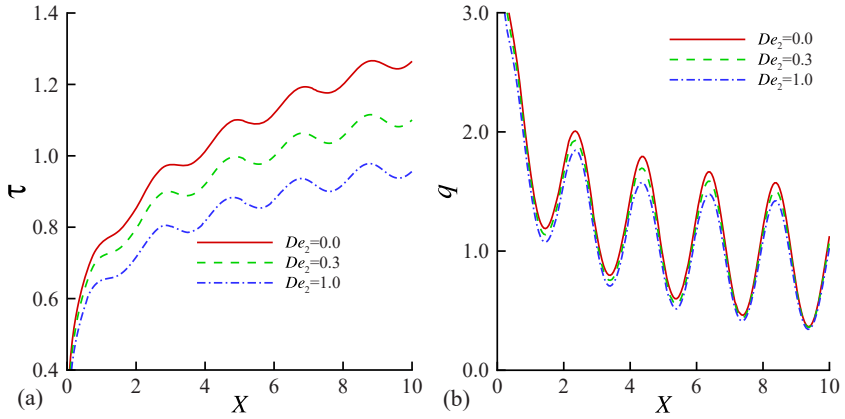

Fig. 4. (a) τ and (b) q for higher De_2, when Pr = 6.2, $a = 0.1$, $\varphi_1 = 0.05$, $\varphi_2 = 0.05$, $De_1 = 0.1$, $\Delta = 0.5$, $Ec = 0.1$, $Rd = 0.5$, and $M = 0.05$.

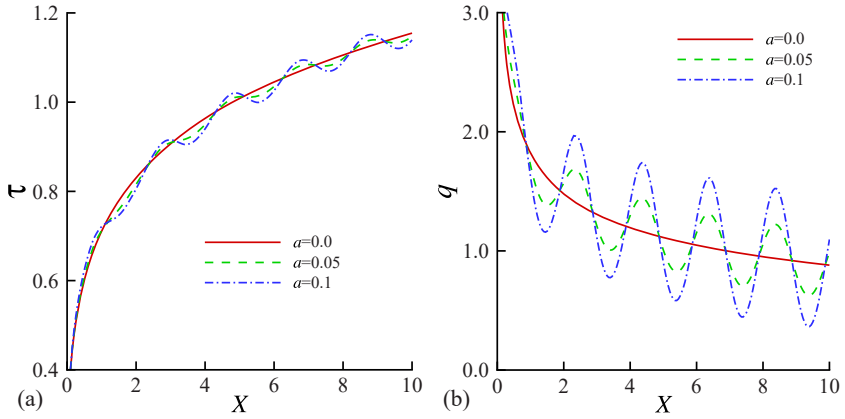

Fig. 5. (a) τ and (b) q for higher a, when Pr = 6.2, $\Delta = 0.5$, $\varphi_1 = 0.05$, $\varphi_2 = 0.05$, $De_1 = 0.1$, $De_2 = 0.2$, $Ec = 0.1$, $Rd = 0.5$, and $M = 0.05$.

temperature that leads to increase the heat transport rate.

In Fig. 7(a)-(b), the influence of Eckert number, Ec, on τ and q are displayed. It is seen that q decreases and τ increases with larger Ec. It is because viscous dissipation increases the temperature near the surface and thereby reduces the temperature gradients at the plate.

Fig. 8(a)-(b) demonstrate the impacts of magnetic field parameters, M, on τ and q. As the existence of magnetic field creates obstacle for the fluid flow, hence, τ show decreasing behavior with the higher M. Furthermore, q showed decreasing behavior when M takes larger values.

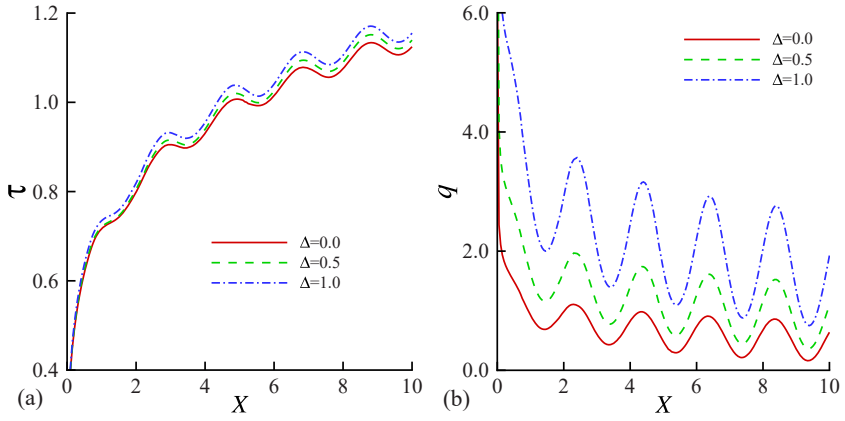

Fig. 6. (a) τ and (b) q for higher Δ, when Pr $= 6.2$, $a = 0.1$, $\varphi_1 = 0.05$, $\varphi_2 = 0.05$, $De_1 = 0.1$, $De_2 = 0.2$, $Ec = 0.1$, $Rd = 0.5$, and $M = 0.05$.

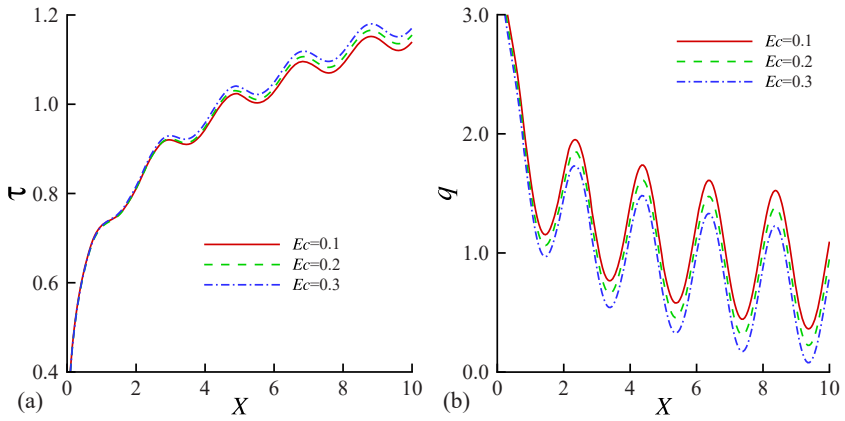

Fig. 7. (a) τ and (b) q for higher Ec, when Pr $= 6.2$, $a = 0.1$, $\varphi_1 = 0.05$, $\varphi_2 = 0.05$, $De_1 = 0.1$, $De_2 = 0.2$, $\Delta = 0.5$, $Rd = 0.5$, and $M = 0.05$.

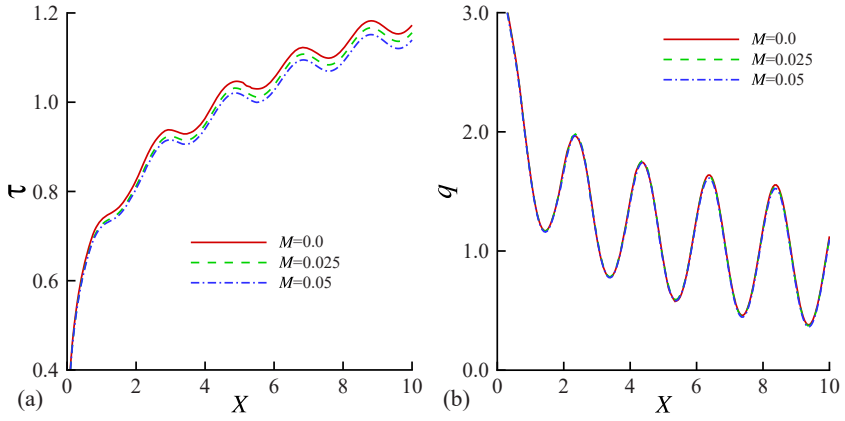

Fig. 8. (a) τ and (b) q for higher M, when Pr $= 6.2$, $\varphi_1 = 0.05$, $\varphi_2 = 0.05$, $De_1 = 0.1$, $De_2 = 0.2$, $Ec = 0.1$, $\Delta = 0.5$, $Rd = 0.5$, and $a = 0.1$.

In Fig. 9(a)-(b), the impacts of Fe_3O_4 nanoparticles, φ_1, on τ and q are discussed. As it is known that, adding more nanoparticles improved q, so the heat transport rate increased for higher φ_1. Since, adding nanoparticles makes the fluid heavier, hence it slows down the fluid velocity. As a result, τ slowly increases with higher φ_1.

Fig. 10(a)-(b) delimitate the influences of Cu nanoparticles, φ_2, on τ and q. More nano-sized particles inclusion into the base fluid augments the thermal conductivity and heat capacity of the fluid. The increasing values of φ_2 enhance q and τ.

Fig. 11(a)-(b) depict the impacts of radiation conduction parameter, Rd, on τ and q. Here, Rd takes three values, $Rd = 0.0$, 0.5, and

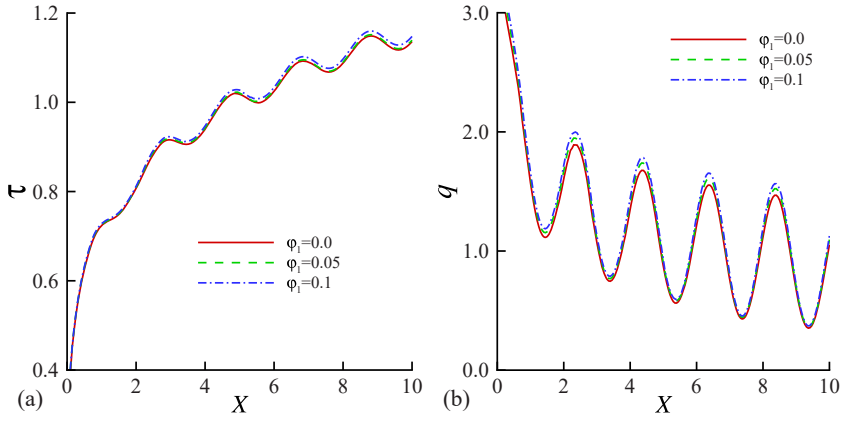

Fig. 9. (a) τ and (b) q for higher φ_1, when Pr = 6.2, $\varphi_2 = 0.05$, $De_1 = 0.1$, $De_2 = 0.2$, $Ec = 0.1$, $\Delta = 0.5$, $Rd = 0.5$, $a = 0.1$, and $M = 0.05$.

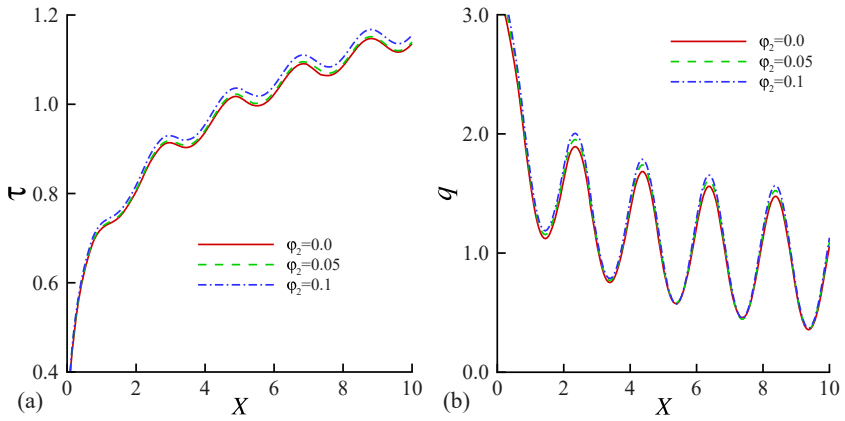

Fig. 10. (a) τ and (b) q for higher φ_2, when Pr = 6.2, $\varphi_1 = 0.05$, $De_1 = 0.1$, $De_2 = 0.2$, $Ec = 0.1$, $\Delta = 0.5$, $Rd = 0.5$, $a = 0.1$ and $M = 0.05$.

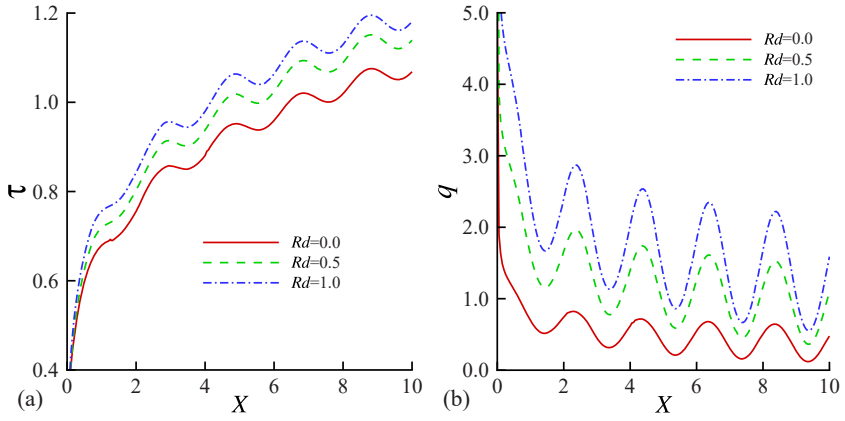

Fig. 11. (a) τ and (b) q for higher Rd, when Pr = 6.2, $\varphi_1 = 0.05$, $\varphi_2 = 0.05$, $De_1 = 0.1$, $De_2 = 0.2$, $Ec = 0.1$, $\Delta = 0.5$, $a = 0.1$ and $M = 0.05$.

1.0. Both profiles show strong changes with higher values of Rd. Both τ and q increases with increasing Rd.

The influences of Deborah number, De_1, on the $\psi(X, Y)$, and $\theta(X, Y)$ are discussed in Fig. 12(a)-(b). With the increase of De_1 the momentum, and thermal boundary are decreased for growing De_1. The impacts of De_1 on momentum boundary are noticeable, but they are small on the thermal boundary.

Fig. 13(a)-(b) depict the impacts of Deborah number, De_2, on $\psi(X, Y)$, and $\theta(X, Y)$. The thermal, and momentum boundary are significantly increased with an increase of De_2. The increasing rate is higher away from the leading corner of the plate compared to the

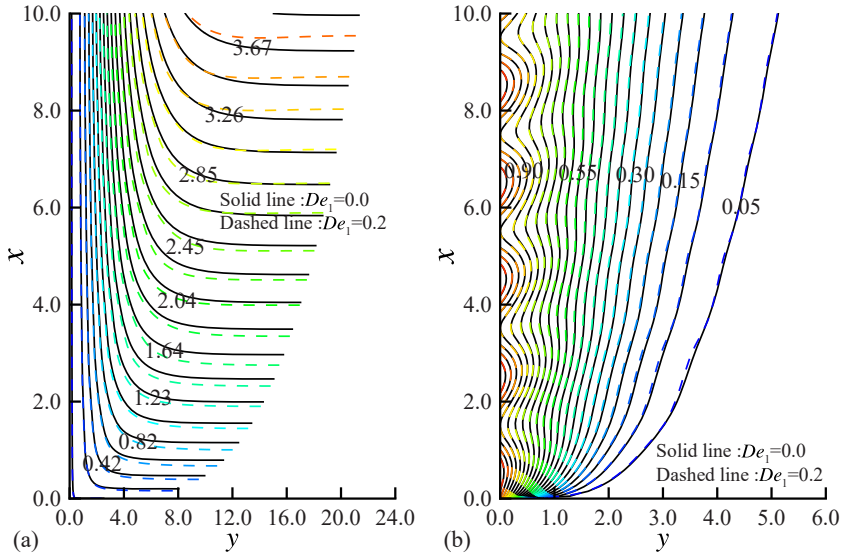

Fig. 12. (a) $\psi(X, Y)$, and (b) $\theta(X, Y)$ for higher De_1, when Pr = 6.2, $\varphi_1 = 0.05$, $\varphi_2 = 0.05$, $De_2 = 0.2$, $\Delta = 0.5$, $Ec = 0.1$, $Rd = 0.5$, $a = 0.1$ and $M = 0.05$.

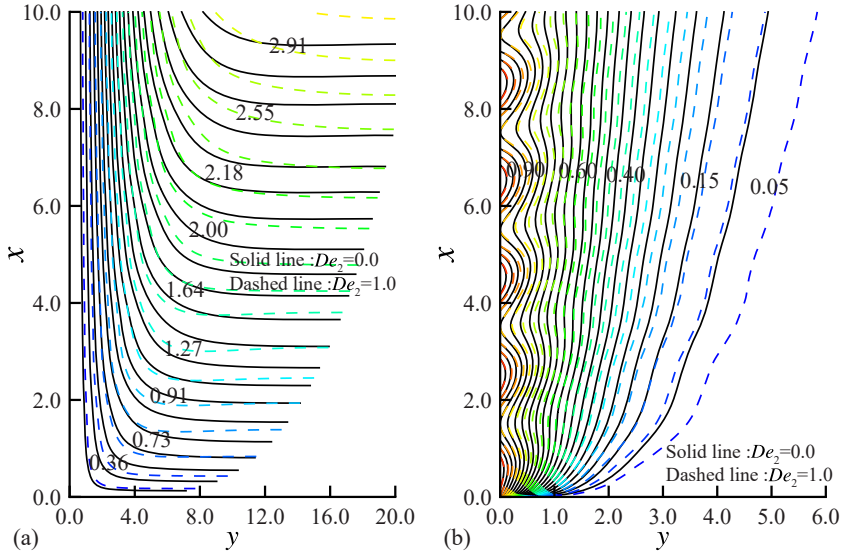

Fig. 13. (a) $\psi(X, Y)$, and (b) $\theta(X, Y)$ for higher De_2, when Pr = 6.2, $\varphi_1 = 0.05$, $\varphi_2 = 0.05$, $De_1 = 0.1$, $\Delta = 0.5$, $Ec = 0.1$, $Rd = 0.5$, $a = 0.1$ and $M = 0.05$.

lower portion flow on the vertical plate.

The effects of surface temperature parameters, Δ, on $\psi(X, Y)$, and $\theta(X, Y)$ are elucidated in Fig. 14(a)-(b). The momentum boundary lessens while thermal boundary enhances with large Δ. For $\Delta = 1.0$, ambient temperature is higher than mean temperature that leads to enhance the heat transfer.

The impacts of radiation conduction parameter, Rd, on $\psi(X, Y)$, and $\theta(X, Y)$ are shown in Fig. 15(a)-(b). In downstream flow, the momentum boundary decreases rapidly, while, away from the leading corner of the vertical plate, the momentum boundary increase. As expected, thermal boundary improve remarkably with an increment in Rd.

Fig. 16(a)-(b) exhibit the influences of Eckert number, Ec, on $\psi(X, Y)$, and $\theta(X, Y)$. The momentum boundary significantly declines with higher Ec. Along the vertical plate, the thermal boundary slowly increases then it starts to gradually increase with higher Ec.

Fig. 17(a)-(b) display the impacts of magnetic parameter, M, on the $\psi(X, Y)$, and $\theta(X, Y)$. Since it is expected that the magnetic field diminishes the velocity of fluid, so the momentum boundary diminishes slowly in downstream region but reduces rapidly on the upper part fluid flow near the plate. Moreover, the thermal boundary slowly decreases with the increase of M.

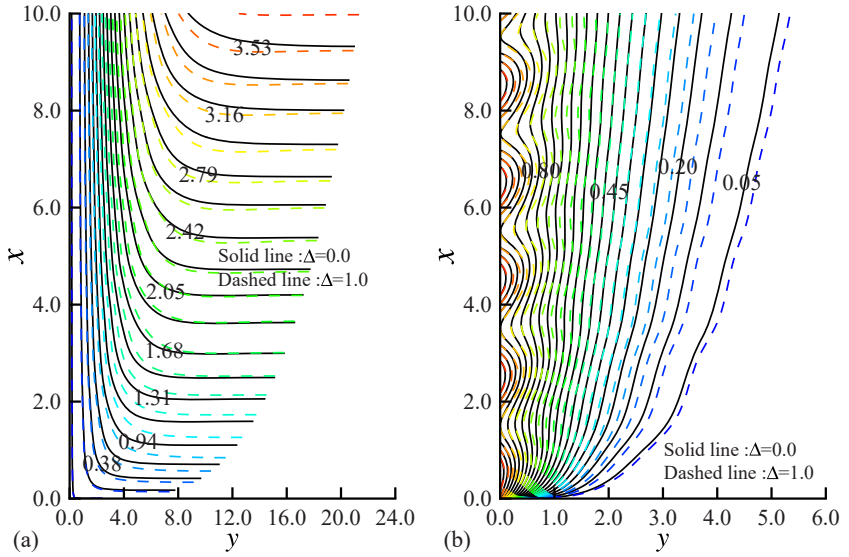

Fig. 14. (a) $\psi(X, Y)$, and (b) $\theta(X, Y)$ for higher Δ, when Pr = 6.2, $\varphi_1 = 0.05$, $\varphi_2 = 0.05$, $De_1 = 0.1$, $De_2 = 0.2$, $Ec = 0.1$, $Rd = 0.5$, $a = 0.1$ and $M = 0.05$.

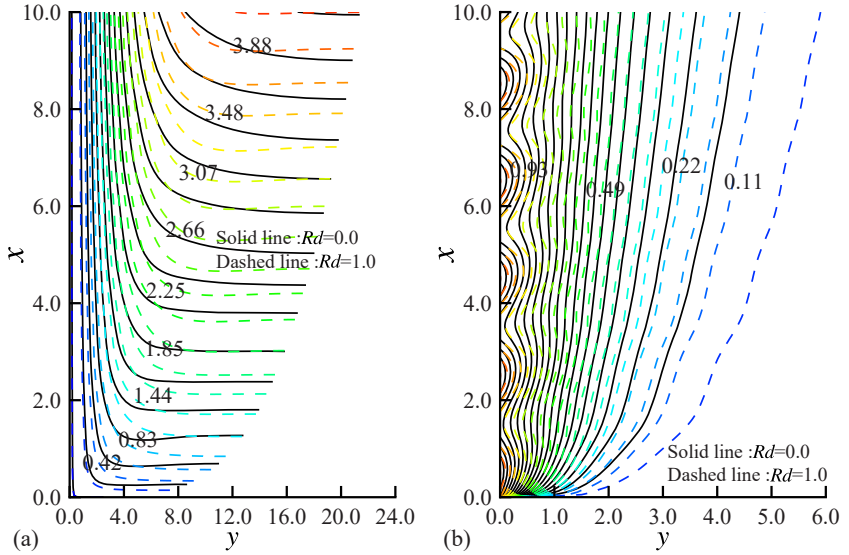

Fig. 15. (a) $\psi(X, Y)$, and (b) $\theta(X, Y)$ for higher Rd, when Pr = 6.2, $\varphi_1 = 0.05$, $\varphi_2 = 0.05$, $De_1 = 0.1$, $De_2 = 0.2$, $Ec = 0.1$, Δ = 0.5, $a = 0.1$ and $M = 0.05$.

The impacts of amplitude of surface temperature, a, on $\psi(X, Y)$, and $\theta(X, Y)$ are exhibited in Fig. 18(a)-(b). Larger values of a remarkably affect the flow of the fluid with decreasing characteristics. But it shows no effect on thermal boundaries along the plate. Away from the plate, the thermal boundary oscillates slightly.

Fig. 19(a)-(b) show the effects of Fe_3O_4 nanoparticles, φ_1, on $\psi(X, Y)$, and $\theta(X, Y)$. Both the momentum, and thermal boundary are increased with an increasing effect of φ_1. In the lower part flow, the momentum boundary increases slowly than upper part flow. This is because, adding more nano-sized particles in base fluid makes the fluid sticky on the plate and considerably increases the thermal conductivity.

Fig. 20(a)-(b) illustrate the impacts of Cu nanoparticles, φ_2, on $\psi(X, Y)$, and $\theta(X, Y)$. The thermal boundary increase with higher φ_2. In the lower part fluid flow along the plate, the momentum boundary increase slowly than the upper part flow. Inclusion of additional nanoparticles in conventional fluids markedly augmented thermal conductivity and heat capacity.

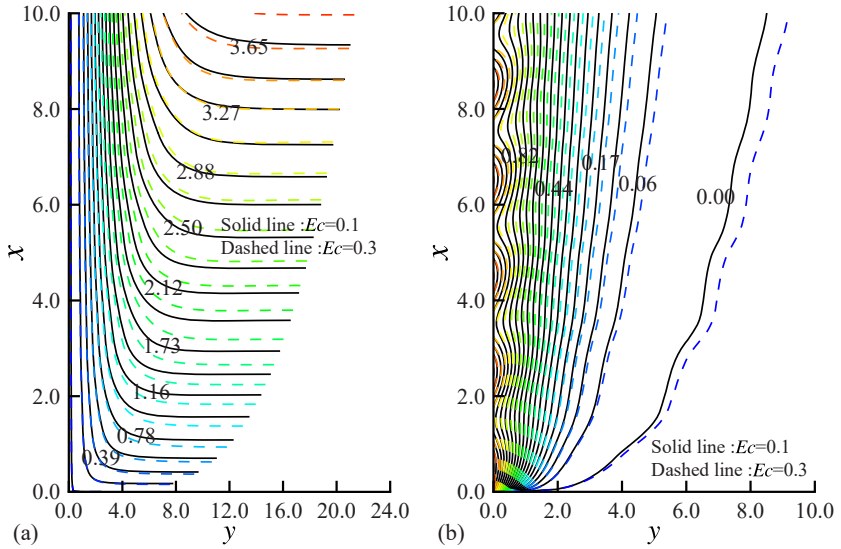

Fig. 16. (a) $\psi(X, Y)$, and (b) $\theta(X, Y)$ for higher Ec, when Pr = 6.2, $\varphi_1 = 0.05$, $\varphi_2 = 0.05$, $De_1 = 0.1$, $De_2 = 0.2$, $\Delta = 0.5$, $Rd = 0.5$, $a = 0.1$ and $M = 0.05$.

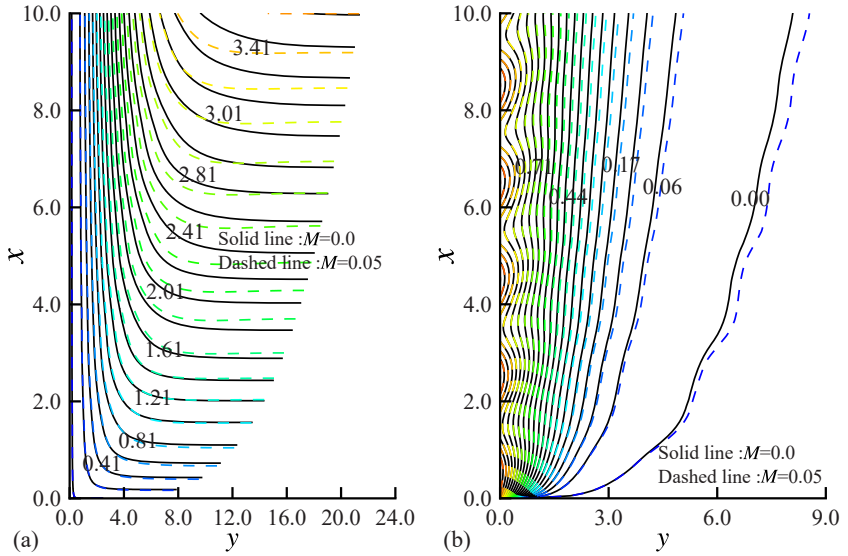

Fig. 17. (a) $\psi(X, Y)$, and (b) $\theta(X, Y)$ for higher M, when Pr = 6.2, $\varphi_1 = 0.05$, $\varphi_2 = 0.05$, $De_1 = 0.1$, $De_2 = 0.2$, $Ec = 0.1$, $\Delta = 0.5$, $Rd = 0.5$, and $a = 0.1$.

5. Conclusions

In the current study, we have studied natural convection viscoelastic second grade fluid flow with variations of sinusoidal surface temperature. Initially, the plate is considered heated. The influences of thermal radiations and magnetic field parameters are also taken. The streamlines and isotherms are also plotted and they give the expected results. The dimensional model equations are modified to non-dimensional form by suitable dimensionless quantities and solved by the finite difference method. Outcomes are showed in graphically for improving effects of several relevant fluid parameters. The inclusion of hybrid nanoparticles into conventional fluids augments q, momentum, and thermal boundary layers. The improving values of radiation conduction parameters and surface temperature parameters augment τ, and q. The increasing values of Eckert numbers boost up τ, but slow down q. Magnetic field parameters hinder the fluid flow and slowly declines q. The larger values of a, make τ, and q oscillating.

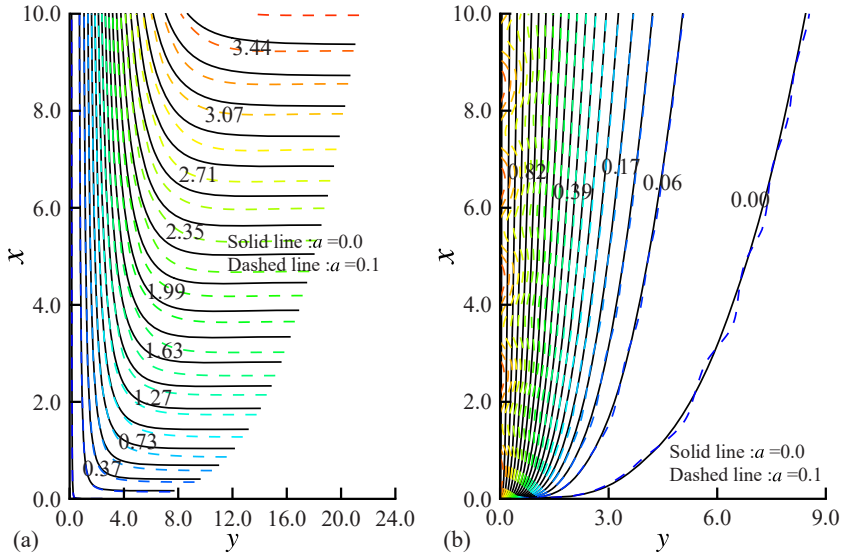

Fig. 18. (a) $\psi(X, Y)$, and (b) $\theta(X, Y)$ for higher a, when Pr = 6.2, $\varphi_1 = 0.05$, $\varphi_2 = 0.05$, $De_1 = 0.1$, $De_2 = 0.2$, $\Delta = 0.5$, $Ec = 0.1$, $Rd = 0.5$, and $M = 0.05$.

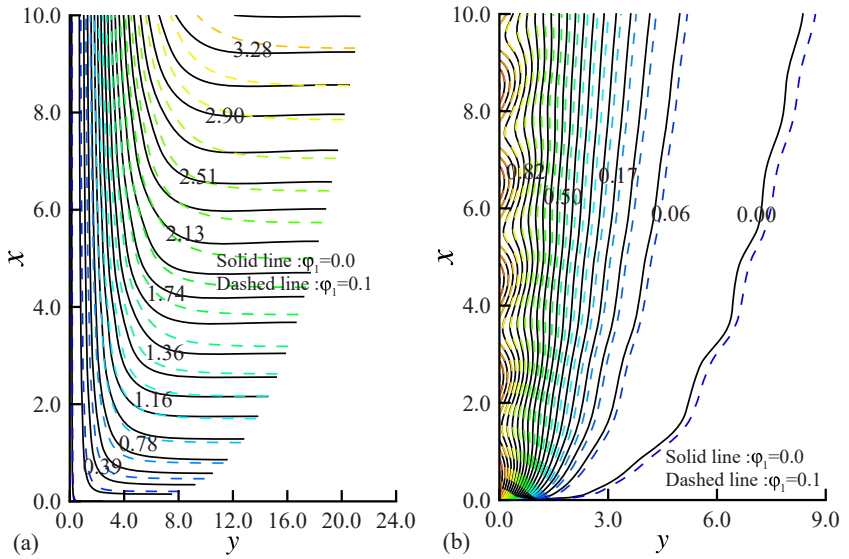

Fig. 19. (a) $\psi(X, Y)$, and (b) $\theta(X, Y)$ higher of φ_1, when Pr = 6.2, $\varphi_2 = 0.05$, $De_1 = 0.1$, $De_2 = 0.2$, $Ec = 0.1$, $\Delta = 0.5$, $Rd = 0.5$, $a = 0.1$ and $M = 0.05$.

Author contribution statement

Nepal Chandra Roy: Conceived and designed the analysis; Analyzed and interpreted the data; Wrote the paper.
Ayantika Ghosh: Analyzed and interpreted the data; Contributed analysis tools or data; Wrote the paper.

Data availability statement

Data will be made available on request.

Declaration of competing interest

The authors declare that they have no known competing financial interests or personal relationships that could have appeared to influence the work reported in this paper.

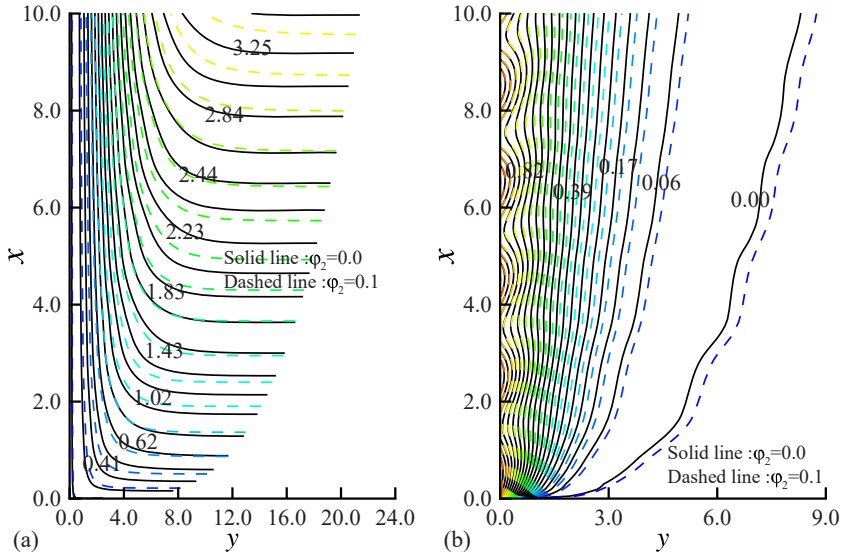

Fig. 20. (a) $\psi(X, Y)$, and (b) $\theta(X, Y)$ for higher φ_2, when Pr = 6.2, $\varphi_1 = 0.05$, $De_1 = 0.1$, $De_2 = 0.2$, $Ec = 0.1$, $\Delta = 0.5$, $Rd = 0.5$, $a = 0.1$ and $M = 0.05$.

Appendix A. Supplementary data

Supplementary data to this article can be found online at https://doi.org/10.1016/j.heliyon.2023.e15703.

References

[1] D.W. Beard, K. Walters, Elastico-viscous boundary-layer flows I. Two-dimensional flow near a stagnation point, Proc. Camb. Phil. Sou. 60 (3) (1964) 667–674, https://doi.org/10.1017/S0305004100038147.
[2] M.M.H. Devies, A Note on Elastico-viscous boundary layer flows, J. Appl. Math. Phys. 17 (1966) 189–191, https://doi.org/10.1007/BF01594096.
[3] K. Vajravelu, D. Rollins, Hydromagnetic flow of a second grade fluid over a stretching sheet, Appl. Math. Comput. 148 (2004) 783–791, https://doi.org/10.1016/S0096-3003(02)00942-6.
[4] M. Turkyilmazoglu, The analytical solution of mixed convection heat transfer and fluid flow of a MHD viscoelastic fluid over a permeable stretching surface, Int. J. Mech. Sci. 77 (2013) 263–268, https://doi.org/10.1016/j.ijmecsci.2013.10.011.
[5] M. Hameed, A.A. Khan, R. Ellahi, M. Raza, Study of magnetic and heat transfer on the peristaltic transport of a fractional second grade fluid in a vertical tube, Int. J. Eng. Sci. Technol. 18 (2015) 496–502, https://doi.org/10.1016/j.jestch.2015.03.004.
[6] M. Khan, M.u. Rahman, Flow and heat transfer to modified second grade fluid over a non-linear stretching sheet, AIP Adv. 5 (2015), 087157, https://doi.org/10.1063/1.4929480.
[7] T. Salahuddin, N. Siddique, M. Khan, M. Altanji, A significant study on flow analysis of viscoelastic fluid with variable thermo-physical properties, Math. Comput. Simulat. 194 (2022) 416–429, https://doi.org/10.1016/j.matcom.2021.11.024.
[8] S.U.S. Choi, Enhancing thermal conductivity of fluids with nanoparticles, 231/MD-Vol. 6, in: D.A. Signier, H.P. Wang (Eds.), Developments and Applications of Non-newtonian Flows, FED-, ASME, New York, 1995, pp. 99–105.
[9] R.K. Tiwari, M.K. Das, Heat transfer augmentation in a two-sided lid-driven differentially heated square cavity utilizing nanofluids, Int. J. Heat Mass Tran. 50 (2007) 2002–2018, https://doi.org/10.1016/j.ijheatmasstransfer.2006.09.034.
[10] H.K. Dawood, H.A. Mohammed, K.M. Munisamy, Heat transfer augmentation using nanofluids in an elliptic annulus with constant heat flux boundary condition, Case Stud. Therm. Eng. 4 (2014) 32–41, https://doi.org/10.1016/j.csite.2014.06.001.
[11] L. Liu, V. Stetsyuk, K.J. Kubiak, Y.F. Yap, A. Goharzadeh, J.C. Chai, Nanoparticles for convective heat transfer enhancement: heat transfer coefficient and the effects of particle size and zeta potential, Chem. Eng. Commun. 206 (2019) 761–771, https://doi.org/10.1080/00986445.2018.1525364.
[12] R. Wang, T. Chen, J. Qi, J. Du, G. Pan, L. Huang, Investigation on the heat transfer enhancement by nanofluid under electric field considering electrophoretic and thermophoretic effect, Case Stud. Therm. Eng. 28 (2021), 101498, https://doi.org/10.1016/j.csite.2021.101498.
[13] T. Grosan, I. Pop, Flow and heat transfer over a permeable biaxial stretching/shrinking sheet in a nanofluid, Neural Comput, Appl 32 (2020) 4575–4582, https://doi.org/10.1007/s00521-018-3770-0.
[14] N.S. Anuar, N. Bachok, N.M. Arifin, H. Rosali, MHD flow past a nonlinear stretching/shrinking sheet in carbon nanotubes: stability analysis, Chin. J. Phys. 65 (2020) 436–446, https://doi.org/10.1016/j.cjph.2020.03.003.
[15] X. Tian, B. Li, Z. Hu, Convective stagnation point flow of a MHD non-Newtonian nanofluid towards a stretching plate, Int. J. Heat Mass Tran. 127 (2018) 768–780, https://doi.org/10.1016/j.ijheatmasstransfer.2018.07.033.
[16] M. Narahari, S.S.K. Raju, R. Pendyala, Unsteady natural convection flow of multi-phase nanofluid past a vertical plate with constant heat flux, Chem. Eng. Sci. 167 (2017) 229–241, https://doi.org/10.1016/j.ces.2017.04.019.
[17] A.M. Hussein, M.M. Noor, K. Kadirgama, D. Ramasamy, M.M. Rahman, Heat transfer enhancement using hybrid nanoparticles in ethylene glycol through a horizontal heated tube, Int. J. Automot. Mech. Eng. 14 (2017) 4183–4195, https://doi.org/10.15282/ijame.14.2.2017.6.0335.
[18] L.A. Lund, Z. Omar, I. Khanb, A.H. Seikh, E.M. Sherif, K.S. Nisar, Stability analysis and multiple solution of Cu–Al_2O_3/H_2O nanofluid contains hybrid nanomaterials over a shrinking surface in the presence of viscous dissipation, J. Mater. Res. Technol. 9 (2020) 421–432, https://doi.org/10.1016/j.jmrt.2019.10.071.
[19] N.A. Zainal, R. Nazar, K. Naganthran, I. Pop, MHD mixed convection stagnation point flow of a hybrid nanofluid past a vertical flat plate with convective boundary condition, Chin. J. Phys. 66 (2020) 630–644, https://doi.org/10.1016/j.cjph.2020.03.022.

[20] M.M. Junoh, F.M. Ali, N.M. Arifin, N. Bachok, I. Pop, MHD stagnation-point flow and heat transfer past a stretching/shrinking sheet in a hybrid nanofluid with induced magnetic field, Int. J. Numer. Methods Heat Fluid Flow 30 (2020) 1345–1364, https://doi.org/10.1108/HFF-06-2019-0500.

[21] A. Mourad, A. Aissa, F. Mebarek-Oudina, W. Jamshed, W. Ahmed, H.M. Ali, A.M. Rashad, Galerkin finite element analysis of thermal aspects of Fe_3O_4-MWCNT/water hybrid nanofluid filled in wavy enclosure with uniform magnetic field effect, Int. Commun. Heat Mass Tran. 126 (2021), 105461, https://doi.org/10.1016/j.icheatmasstransfer.2021.105461.

[22] K. Gangadhar, M.A. Kumari, A.J. Chamkha, EMHD flow of radiative second-grade nanofuid over a riga plate due to convective heating: revised Buongiorno's nanofuid model, Arabian J. Sci. Eng. 47 (2022) 8093–8103, https://doi.org/10.1007/s13369-021-06092-7.

[23] R.S.V. Kumar, R.J.P. Gowda, R.N. Kumar, M. Radhika, B.C. Prasannakumara, Two-phase flow of dusty fluid with suspended hybrid nanoparticles over a stretching cylinder with modified Fourier heat flux, SN Appl. Sci. 3 (2021) 384, https://doi.org/10.1007/s42452-021-04364-3.

[24] S. Jakeer, P.B. Reddy, A.M. Rashad, H.A. Nabwey, Impact of heated obstacle position on magneto-hybrid nanofluid flow in a lid-driven porous cavity with Cattaneo-Christov heat flux pattern, Alex. Eng. J. 60 (2021) 821–835, https://doi.org/10.1016/j.aej.2020.10.011.

[25] G. Kotha, V.R. Kolipaula, M.V.S. Rao, S. Penki, A.J. Chamkha, Internal heat generation on bioconvection of an MHD nanofluid flow due to gyrotactic microorganisms, Eur. Phys. J. Plus 135 (2020) 600, https://doi.org/10.1140/epjp/s13360-020-00606-2.

[26] K. Sarada, F. Gamaoun, A. Abdulrahman, S.O. Paramesh, R. Kumar, G.D. Prasanna, R.J.P. Gowda, Impact of exponential form of internal heat generation on water-based ternary hybrid nanofluid flow by capitalizing non-Fourier heat flux model, Case Stud. Therm. Eng. 38 (2022), 102332, https://doi.org/10.1016/j.csite.2022.102332.

[27] A. Mahdy, E.R. El-Zahar, A.M. Rashad, W. Saad, H.S. Al-Juaydi, The magneto-natural convection flow of a micropolar hybrid nanofluid over a vertical plate saturated in a porous medium, Fluids 6 (2021) 202, https://doi.org/10.3390/fluids6060202.

[28] K. Gangadhar, M.A. Kumari, M.V.S. Rao, A.J. Chamkha, Oldroyd-B nanoliquid flow through a triple stratified medium submerged with gyrotactic bioconvection and nonlinear radiations, Arabian J. Sci. Eng. 47 (2022) 8863–8875, https://doi.org/10.1007/s13369-021-06412-x.

[29] R.J.P. Gowda, R.N. Kumar, A.M. Jyothi, B.C. Prasannakumara, K.S. Nisar, KKL correlation for simulation of nanofluid flow over a stretching sheet considering magnetic dipole and chemical reaction, Z. Angew. Math. Mech. 101 (2021), e202000372, https://doi.org/10.1002/zamm.202000372.

[30] K. Gangadhar, R.E. Nayak, M.V.S. Rao, T. Kannan, Nodal/Saddle stagnation point slip flow of an aqueous convectional magnesium oxide–gold hybrid nanofuid with viscous dissipation, Arabian J. Sci. Eng. 46 (2021) 2701–2710, https://doi.org/10.1007/s13369-020-05195-x.

[31] K.S. Nisar, R. Mohapatra, S.R. Mishra, M.G. Reddy, Semi-analytical solution of MHD of free convective Jeffrey fluid flow in the presence of heat source and chemical reaction, Ain Shams Eng. J. 12 (2021) 837–845, https://doi.org/10.1016/j.asej.2020.08.015.

[32] K. Ahmad, A. Ishak, Magnetohydrodynamic (MHD) Jeffrey fluid over a stretching vertical surface in a porous medium, Propuls. Power Res. 6 (2017) 269–276, https://doi.org/10.1016/j.jppr.2017.11.007.

[33] T. Hayat, N. Ahmad, N. Ali, Effects of an endoscope and magnetic field on the peristalsis involving Jeffrey fluid, Commun. Nonlinear Sci. Numer. Simul. 13 (2008) 1581–1591, https://doi.org/10.1016/j.cnsns.2007.02.008.

[34] A. Alsaedi, Z. Iqbal, M. Mustafa, T. Hayat, Exact solutions for the magnetohydrodynamic flow of a Jeffrey fluid with convective boundary conditions and chemical reaction, Z. Naturforsch. 67a (2012) 517–524, https://doi.org/10.5560/zna.2012-0054.

[35] M. Turkyilmazoglu, I. Pop, Exact analytical solutions for the flow and heat transfer near the stagnation point on a stretching/shrinking sheet in a Jeffrey fluid, Int. J. Heat Mass Tran. 57 (2013) 82–88, https://doi.org/10.1016/j.ijheatmasstransfer.2012.10.006.

[36] M. Haneef, H.A. Madkhali, A. Salmi, S.O. Alharbi, M.Y. Malik, Numerically study on heat and mass transfer in Maxwell fluid with tri and hybrid nanoparticles, Int. Commun. Heat Mass Tran. 135 (2022), 106061, https://doi.org/10.1016/j.icheatmasstransfer.2022.106061.

[37] H. Hanif, A computational approach for boundary layer flow and heat transfer of fractional Maxwell fluid, Math. Comput. Simulat. 191 (2022) 1–13, https://doi.org/10.1016/j.matcom.2021.07.024.

[38] R.N. Kumar, A.M. Jyothi, H. Alhumade, R.J.P. Gowda, M.M. Alam, I. Ahmad, M.R. Gorji, B.C. Prasannakumara, Impact of magnetic dipole on thermophoretic particle deposition in the flow of Maxwell fluid over a stretching sheet, J. Mol. Liq. 334 (2021), 116494, https://doi.org/10.1016/j.molliq.2021.116494.

[39] W. Jamshed, Numerical investigation of MHD impact on Maxwell nanofluid, Int. Commun. Heat Mass Tran. 120 (2021), 104973, https://doi.org/10.1016/j.icheatmasstransfer.2020.104973.

[40] X. Zhang, R. Shah, S. Saleem, N.A. Shah, Z.A. Khan, J.D. Chung, Natural convection flow Maxwell fluids with generalized thermal transport and Newtonian heating, Case Stud. Therm. Eng. 27 (2021), 101226, https://doi.org/10.1016/j.csite.2021.101226.

[41] I. Khan, A. Raza, M.A. Shakir, A.S. Al-Johani, A.A. Pasha, K. Irshad, Natural convection simulation of Prabhakar-like fractional Maxwell fluid flowing on inclined plane with generalized thermal flux, Case Stud. Therm. Eng. 35 (2022), 102042, https://doi.org/10.1016/j.csite.2022.102042.

[42] C. Fetecau, C. Fetecau, A new exact solution for the flow of a Maxwell fluid past an infinite plate, Int. J. Non Lin. Mech. 38 (2003) 423–427, https://doi.org/10.1016/S0020-7462(01)00062-2.

[43] M. Haneef, M. Nawaz, S.O. Alharbi, Y. Elmasry, Cattaneo-Christov heat flux theory and thermal enhancement in hybrid nano Oldroyd-B rheological fluid in the presence of mass transfer, Int. Commun. Heat Mass Tran. 126 (2021), 105344, https://doi.org/10.1016/j.icheatmasstransfer.2021.105344.

[44] T. Hayat, S.A. Khan, M.I. Khan, S. Momani, A. Alsaedi, Cattaneo-Christov (CC) Heat flux model for nanomaterial stagnation point flow of Oldroyd-B fluid, Comput. Methods Progr. Biomed. 187 (2020), 105247, https://doi.org/10.1016/j.cmpb.2019.105247.

[45] S. Hina, M. Munir, M. Mustafa, A non-Fourier heat flux approach to model MHD Oldroyd-B fluid flow due to bidirectional stretching surface, Int. J. Mech. Sci. 131–132 (2017) 146–154, https://doi.org/10.1016/j.ijmecsci.2017.06.051.

[46] A.U. Awan, M. Ali, K.A. Abro, Electroosmotic slip flow of Oldroyd-B fluid between two plates with non-singular kernel, J. Comput. Appl. Math. 376 (2020), 112885, https://doi.org/10.1016/j.cam.2020.112885.

[47] Y. Liu, L. Zheng, X. Zhang, Unsteady MHD Couette flow of a generalized Oldroyd-B fluid with fractional derivative, Comput. Math. Appl. 61 (2011) 443–450, https://doi.org/10.1016/j.camwa.2010.11.021.

[48] W. Ibrahim, G. Gadisa, Finite element solution of nonlinear convective flow of Oldroyd-B fluid with Cattaneo-Christov heat flux model over nonlinear stretching sheet with heat generation or absorption, Propuls. Power Res. 9 (2020) 304–315, https://doi.org/10.1016/j.jppr.2020.07.001.

[49] M. Qasim, Heat and mass transfer in a Jeffrey fluid over a stretching sheet with heat source/sink, Alex. Eng. J. 52 (2013) 571–575, https://doi.org/10.1016/j.aej.2013.08.004.

[50] S.M. Mahfooz, M.A. Hossain, Conduction-radiation effect on transient natural convection with thermophoresis, Appl. Math. Mech. 33 (2012) 271–288, https://doi.org/10.1007/s10483-012-1549-6.

[51] S.A. Shehzad, A. Alsaedi, T. Hayat, Influence of thermophoresis and joule heating on the radiative flow of Jeffrey fluid with mixed convection, Braz. J. Chem. Eng. 30 (2013) 897–908, https://doi.org/10.1590/S0104-66322013000400021.

[52] O. Aydın, A. Kaya, Radiation effect on MHD mixed convection flow about a permeable vertical plate, Heat Mass Tran. 45 (2008) 239–246, https://doi.org/10.1007/s00231-008-0428-y.

[53] M.M. Rashidi, B. Rostami, N. Freidoonimehr, S. Abbasbandy, Free convective heat and mass transfer for MHD fluid flow over a permeable vertical stretching sheet in the presence of the radiation and buoyancy effects, Ain Shams Eng. J. 5 (2014) 901–912, https://doi.org/10.1016/j.asej.2014.02.007.

[54] J. Wang, M.I. Khan, W.A. Khan, S.Z. Abbas, M.I. Khan, Transportation of heat generation/absorption and radiative heat flux in homogeneous–heterogeneous catalytic reactions of non-Newtonian fluid (Oldroyd-B model), Comput. Methods Progr. Biomed. 189 (2020), 105310, https://doi.org/10.1016/j.cmpb.2019.105310.

[55] A. Wakif, A. Chamkha, T. Thumma, I.L. Animasaun, R. Sehaqui, Thermal radiation and surface roughness efects on the thermo-magneto-hydrodynamic stability of alumina–copper oxide hybrid nanofuids utilizing the generalized Buongiorno's nanofuid model, J. Therm. Anal. Calorim. 143 (2021) 1201–1220, https://doi.org/10.1007/s10973-020-09488-z.

[56] S. Siddiqa, N. Begum, T. Iftikhar, M. Rafiq, M.A. Hossain, R.S.R. Gorla, Thermal radiation effects on Casson dusty boundary-layer fluid flow along an isothermal truncated vertical cone, Arabian J. Sci. Eng. 44 (2019) 7833–7842, https://doi.org/10.1007/s13369-019-03915-6.

[57] B.J. Akinbo, B.I. Olajuwon, Impact of radiation and chemical reaction on stagnation-point flow of Hydromagnetic Walters' B fluid with Newtonian heating, Int. Commun. Heat Mass Tran. 121 (2021), 105115, https://doi.org/10.1016/j.icheatmasstransfer.2021.105115.
[58] L. Ali, X. Liu, B. Ali, S. Mujeed, S. Abdal, Finite element analysis of thermo-diffusion and multi-slip effects on MHD unsteady flow of Casson nano-fluid over a shrinking/stretching sheet with radiation and heat source, Appl. Sci. 9 (2019) 5217, https://doi.org/10.3390/app9235217.
[59] A. Jamaludin, K. Naganthran, R. Nazar, I. Pop, MHD mixed convection stagnation-point flow of Cu-Al_2O_3/water hybrid nanofluid over a permeable stretching/shrinking surface with heat source/sink, Eur. J. Mech. B Fluid 84 (2020) 71–80, https://doi.org/10.1016/j.euromechflu.2020.05.017.
[60] D.A.S. Rees, The effect of steady streamwise surface temperature variations on vertical free convection, Int. J. Heat Mass Tran. 42 (1999) 2455–2464, https://doi.org/10.1016/S0017-9310(98)00304-4.
[61] N.C. Roy, M.A. Hossain, Numerical solution of a steady natural convection flow from a vertical plate with the combined effects of streamwise temperature and species concentration variations, Heat Mass Tran. 46 (2010) 509–522, https://doi.org/10.1007/s00231-010-0591-9.
[62] M.M. Molla, S.C. Saha, M.A. Hossain, Radiation effect on free convection laminar flow along a vertical flat plate with streamwise sinusoidal surface temperature, Math. Comput. Model. 53 (2011) 1310–1319, https://doi.org/10.1016/j.mcm.2010.12.017.
[63] N. Chen, F. Wang, R. Hu, M.A. Hossain, Compressibility effect on natural convection flow along a vertical plate with isotherm and streamwise sinusoidal surface temperature, Int. J. Heat Mass Tran. 99 (2016) 738–749, https://doi.org/10.1016/j.ijheatmasstransfer.2016.04.025.
[64] A. Ghaffari, T. Javed, K. Hsiao, Heat transfer analysis of unsteady oblique stagnation point flow of elastico-viscous fluid due to sinusoidal wall temperature over an oscillating-stretching surface: a numerical approach, J. Mol. Liq. 219 (2016) 748–755, https://doi.org/10.1016/j.molliq.2016.04.014.
[65] N.C. Roy, Magnetohydrodynamic natural convection flow of a nanofluid due to sinusoidal surface temperature variations, Phys. Fluids 32 (2020), 022003, https://doi.org/10.1063/1.5143516.
[66] H.R. Ashorynejad, A. Shahriari, MHD natural convection of hybrid nanofluid in an open wavy cavity, Res. Phys. 9 (2018) 440–455, https://doi.org/10.1016/j.rinp.2018.02.045.
[67] M. Gholinia, S. Gholinia, Kh Hosseinzadeh, D.D. Ganji, Investigation on ethylene glycol nano fluid flow over a vertical permeable circular cylinder under effect of magnetic field, Res. Phys. 9 (2018) 1525–1533, https://doi.org/10.1016/j.rinp.2018.04.070.
[68] F.G. Blottner, Finite-difference methods of solution of the boundary layer equations, AIAA J. 8 (1970) 193–205, https://doi.org/10.2514/3.5642.